B17

# Vertex-centred Discretization of Multiphase Compositional Darcy Flows on General Meshes

R. Eymard (University Paris East), C. Guichard* (University of Nice Sophia Antipolis), R. Herbin (University of Provence), R. Masson (University of Nice Sophia Antipolis) & P. Samier (Total)

## SUMMARY

This paper introduces a vertex centred discretization on general 3D meshes of multiphase Darcy flows in heterogeneous anisotropic porous media.
The model accounts for the coupling of the mass balance of each component with the pore volume conservation and the thermodynamical equilibrium.
The conservative spatial discretization of the Darcy fluxes is based on the Vertex Approximate Gradient scheme (VAG) which is unconditionally coercive for arbitrary meshes and permeability tensors.
The stencil of this vertex-centred scheme typically comprises 27 points on topologically Cartesian meshes. On tetrahedral meshes, the number of unknowns is considerably reduced, by typically a factor five, compared with usual cell-centred MultiPoint Fluxes Approximations, which is a key asset for multiphase flow simulations on unstructured meshes.
An adaptive choice of the pore volume at the vertices ensures the accuracy of the discretization even for coarse meshes on highly heterogeneous media.
This approach can easily be implemented on existing reservoir simulators using a graph of transmissibilities for the computation of the fluxes.
The efficiency of our approach is exhibited on several two phase and three phase Darcy flow examples. In particular it includes the nearwell injection of miscible CO2 in a saline aquifer taking into account the precipitation of salt.

## Introduction

Many applications require the simulation of compositional multiphase Darcy flow in heterogeneous porous media. In oil reservoir modelling, the compositional triphase Darcy flow simulator is a key tool to predict and optimize the production of a reservoir. In sedimentary basin modelling, such models are used to simulate the migration of the oil and gas phases in a basin saturated with water at geological space and time scales. The objectives are to predict the location of the potential reservoirs as well as the quality and quantity of oil trapped therein. In $CO_2$ geological storage, compositional multiphase Darcy flow models are used to optimize the injection of $CO_2$ and to assess the long term integrity of the storage. The numerical simulation of such models is a complex task, which has been the object of several works over a long period of time, see the reference books [7] and [21]. Several types of numerical schemes have been proposed in the past decades. Those which are implemented in industrial codes are mainly built upon cell centred approximations and discrete fluxes, in a framework which is also that of the method we propose here. Let us briefly sketch this framework.

The 3D simulation domain $\Omega$ is meshed by control volumes $X \in \mathscr{G}$. Let us denote by $\Lambda$ the diffusion matrix (which is a possibly full matrix depending on the point of the domain). For each control volume $X \in \mathscr{G}$, the set of neighbours $Y \in \mathscr{N}_X$ is the set of all control volumes involved in the mass balance in $X$, which means that the following approximation formula is used:

$$-\int_X \operatorname{div}(\Lambda \nabla p)\,\mathrm{d}x \;\simeq \sum_{Y \in \mathscr{N}_X} F_{X,Y}(P),$$

where $P = (p_Z)_{Z \in \mathscr{G}}$ is the family of all pressure unknowns in the control volumes, and where the flux $F_{X,Y}(P)$, between control volumes $X$ and $Y$, is a linear function of the components of $P$ which ensures the following conservativity property:

$$F_{X,Y}(P) = -F_{Y,X}(P). \tag{1}$$

Such a linear function, which is expected to vanish on constant families, may be defined by

$$F_{X,Y}(P) = \sum_{Z \in \mathscr{G}_{X,Y}} a^Z_{X,Y} p_Z, \tag{2}$$

where the family $(a^Z_{X,Y})_{Z \in \mathscr{G}_{X,Y}}$ and $\mathscr{G}_{X,Y} \subset \mathscr{G}$ are such that $\sum_{Z \in \mathscr{G}_{X,Y}} a^Z_{X,Y} = 0$. We then consider a compositional multiphase Darcy flow, with $N_\alpha$ phases and $N_c$ constituents, the discrete balance law in $X \in \mathscr{G}$ is written

$$\begin{aligned} &\frac{\Phi_X}{\delta t}(A^{(n+1)}_{X,i} - A^{(n)}_{X,i}) + \sum_{\alpha=1}^{N_\alpha} \sum_{Y \in \mathscr{N}_X} M^{(n+1),\alpha}_{X,Y,i} F^{(n+1),\alpha}_{X,Y} = 0, \quad \forall i = 1,\dots,N_c, \\ &F^{(n+1),\alpha}_{X,Y} = F_{X,Y}(P^{(n+1),\alpha}) - \rho^{(n+1),\alpha}_{X,Y} \mathbf{g} \cdot (x_Y - x_X), \quad \forall \alpha = 1,\dots,N_\alpha, \end{aligned} \tag{3}$$

where $n$ is the time index, $\delta t$ is the time step, $\Phi_X$ is the porous volume of the control volume $X$, $A_{X,i}$ represents the accumulation of constituent $i$ in the control volume $X$ per unit pore volume (assumed to take into account the dependence of the porosity with respect to the pressure), $M^\alpha_{X,Y,i}$ is the amount of constituent $i$ transported by phase $\alpha$ from the control volume $X$ to the control volume $Y$ (generally computed by taking the upstream value with respect to the sign of $F^\alpha_{X,Y}$), $P^\alpha$ is the family of the pressure unknowns of phase $\alpha$, $\mathbf{g}$ is the gravity acceleration, $\rho^\alpha_{X,Y}$ is the bulk density of phase $\alpha$ between control volumes $X$ and $Y$ and $x_X$ is the centre of control volume $X$. In addition to these relations, the differences between the phase pressures are ruled by capillary pressure laws. Thermodynamical equilibrium and standard closure relations are used. A more detailed description of this model is described, for example in [17].

The main drawback of cell-centred finite volume schemes is the difficulty to use them in the case of complex meshes and heterogeneous anisotropic permeabilities, which are unfortunately frequently encountered in practice to represent the basin and reservoir geometries and petrophysical properties. Many

progresses have been done during the last decade, leading to the design of cell-centred schemes which remain consistent in such situations. Among these, let us mention for example the well-known O scheme introduced in [1, 2, 10, 11], the L scheme [3], or the SUSHI scheme [14]. We also refer to [4, 5, 6] for the convergence analysis of cell-centred schemes in a general framework. Nevertheless it is still a challenge to design a cell-centred discretization of diffusive fluxes in the case of general meshes and heterogeneous anisotropic diffusion tensors, which is linear, unconditionally coercive and "compact", in the sense that the expression of the discrete flux at a given face of the mesh may at most involve the cells sharing a vertex with this face. For example the O and L schemes are compact but their coercivity is mesh and permeability tensor dependent. On the other hand, the SUSHI scheme is unconditionally coercive but its stencil is not compact, since it involves the neighbours of the neighbours of a given control volume.

Alternately to cell centred schemes, vertex centred schemes, such as the CVFE (Control Volume Finite Element, see for example [12, 9, 20]), are more adapted to unstructured meshes such as tetrahedral meshes and can lead in some cases to coercive schemes. The main difficulty of vertex centred schemes lies in the definition of the rock properties in the case of heterogeneous media. Indeed, assuming that the control volumes are vertex centred with vertices located at the interfaces between different media, then the porous volume concerned by the flow of very permeable medium includes that of non permeable medium. This may lead to surprisingly wrong results on the components velocities. A possible interpretation of these poor results is that, when seen as a set of discrete balance laws, the finite element discretization provides the same amount of impermeable and permeable porous volume for the accumulation term for a node located at a heterogeneous interface.

We present in this paper the use of a new scheme, called Vertex Approximate Gradient (VAG) scheme [15, 16] which try to overcome the above difficulties. The key idea is to use both cell and vertex unknowns in order to obtain and unconditionally coercive scheme on general polyhedral meshes. The VAG scheme can be implemented in (3) so that the components velocities are correctly approximated, thanks to a special choice of the control volumes and of the discrete fluxes, which respect the form (2). The purpose of respecting the form (1)-(3) is to be able to easily plug it into an existing reservoir code, say Multi-Point Flux Approximation (MPFA), by simply redefining the control volumes and the coefficients $a^Z_{X,Y}$ of the discrete flux. Although this scheme is mainly vertex centred, we show that the solution obtained on a very heterogeneous medium with a coarse mesh remains accurate. This is a great advantage of this scheme, which is also consistent, unconditionally coercive, symmetric, and leads to a 27-stencil on hexahedral structured meshes since the cell unknowns can be eliminated locally without any fill-in. In addition the VAG scheme is very efficient, in terms of CPU time, on meshes with tetrahedra as illustrated in the numerical examples.

The outline of the paper is the following. Section one recalls the construction of the VAG scheme for diffusive equations. Then, the VAG scheme fluxes are derived and used in to discretize the compositional multiphase Darcy flow model (3), and the pore volume assignment procedure is detailed. Finally, the second section exhibits the efficiency of the VAG discretization which is compared to the solutions obtained with the MPFA O scheme. The first test cases deal with two phase flow examples including highly heterogeneous cases and discontinuous capillary pressures. Then, the last test case considers the nearwell injection of miscible $CO_2$ in a saline aquifer, taking into account the vaporization of $H_2O$ in the gas phase as well as the precipitation of salt.

**Presentation of the VAG scheme**

Recently, a new discretization of diffusive equations, the Vertex Approximate Gradient (VAG) scheme has been introduced in [15, 16]. In addition to its properties listed in the introduction, it is exact on cellwise affine solutions for cellwise constant diffusion tensors. Moreover it has exhibited a very good compromise between accuracy, robustness and CPU time in the recent FVCA6 3D benchmark [19]. Thus its use for compositional multiphase Darcy flow model (3) was a natural question to study and for

which an answer is given in the following section.

We consider the following diffusion equation,

$$\begin{cases} -\mathrm{div}\,(\Lambda\nabla\bar{u}) = f & \text{in } \Omega, \\ \bar{u} = u^D & \text{on } \partial\Omega, \end{cases}$$

and its variational formulation: which reads find $\bar{u} \in H^1(\Omega)$ such that $\bar{u} = u^D$ on $\partial\Omega$, and

$$\int_\Omega \Lambda\nabla\bar{u}\cdot\nabla v\,dx = \int_\Omega f\,v\,dx$$

for all $v \in H^1_0(\Omega) = \{w \in H^1(\Omega)\,|\,w = 0 \text{ on } \partial\Omega\}$, admits a unique solution $\bar{u}$ provided that the measure of $\partial\Omega$ is nonzero, that $f \in L^2(\Omega)$ and $u^D \in H^{1/2}(\partial\Omega)$, which is assumed in the following. Note that the case of inhomogeneous Neumann boundary condition is detailed for example in [18, 17] and not detailed here for sake of simplicity.

*Discrete framework of the VAG scheme*

Following [16], we consider $\mathscr{M}$ a general polyhedral mesh of $\Omega$ defined by a set of cells $K$ that are disjoint open subsets of $\Omega$ such that $\bigcup_{K\in\mathscr{M}} \bar{K} = \overline{\Omega}$. For all $K \in \mathscr{M}$, $x_K$ denotes the so-called "centre" of the cell $K$ under the assumption that $K$ is star-shaped with respect to $x_K$. Let $\mathscr{F}$ denote the set of faces of the mesh which are not assumed to be planar, hence the term "generalized polyhedral cells". We denote by $\mathscr{V}$ the set of vertices of the mesh. Let $\mathscr{V}_K$, $\mathscr{F}_K$, $\mathscr{V}_\sigma$ respectively denote the set of the vertices of $K \in \mathscr{M}$, faces of $K$, and vertices of $\sigma \in \mathscr{F}$. For any face $\sigma \in \mathscr{F}_K$, we have $\mathscr{V}_\sigma \subset \mathscr{V}_K$. Let $\mathscr{M}_\mathbf{s}$ denote the set of the cells sharing the vertex $\mathbf{s}$. The set of edges of the mesh is denoted by $\mathscr{E}$ and $\mathscr{E}_\sigma$ denotes the set of edges of the face $\sigma \in \mathscr{F}$. It is assumed that, for each face $\sigma \in \mathscr{F}$, there exists a so-called "centre" of the face $x_\sigma$ such that

$$x_\sigma = \sum_{\mathbf{s}\in\mathscr{V}_\sigma} \beta_{\sigma,\mathbf{s}}\,\mathbf{s}, \text{ with } \sum_{\mathbf{s}\in\mathscr{V}_\sigma} \beta_{\sigma,\mathbf{s}} = 1,$$

where $\beta_{\sigma,\mathbf{s}} \geq 0$ for all $\mathbf{s} \in \mathscr{V}_\sigma$. The face $\sigma$ is assumed to match with the union of the triangles $T_{\sigma,e}$ defined by the face centre $x_\sigma$ and each of its edge $e \in \mathscr{E}_\sigma$. Let $\mathscr{V}_{int} = \mathscr{V} \setminus \partial\Omega$ denote the set of interior vertices, and $\mathscr{V}_{ext} = \mathscr{V} \cap \partial\Omega$ the set of boundary vertices.

The previous discretization is denoted by $\mathfrak{D}$ and we define the discrete space

$$\widehat{W}_\mathfrak{D} = \{v_K \in \mathbb{R}, v_\mathbf{s} \in \mathbb{R}, \text{ for } K \in \mathscr{M} \text{ and } \mathbf{s} \in \mathscr{V}\},$$

and its subspace with homogeneous Dirichlet boundary conditions on $\mathscr{V}_{ext}$

$$W_\mathfrak{D} = \{v \in \widehat{W}_\mathfrak{D}\,|\,v_\mathbf{s} = 0 \text{ for } \mathbf{s} \in \mathscr{V}_{ext}\}.$$

The VAG scheme introduced in [16] is based on a piecewise constant discrete gradient reconstruction for functions in the space $\widehat{W}_\mathfrak{D}$. Several constructions are proposed based on different decompositions of the cell. Let us recall the simplest one based on a conforming finite element discretization on a tetrahedral sub-mesh, and we refer to [16, 15] for two other constructions sharing the same basic features.

For all $\sigma \in \mathscr{F}$, the operator $I_\sigma : \widehat{W}_\mathfrak{D} \to \mathbb{R}$ such that

$$I_\sigma(v) = \sum_{\mathbf{s}\in\mathscr{V}_\sigma} \beta_{\sigma,\mathbf{s}} v_\mathbf{s},$$

is by definition of $x_\sigma$ a second order interpolation operator at point $x_\sigma$.

Let us introduce the tetrahedral sub-mesh

$$\mathscr{T} = \{T_{K,\sigma,e} \text{ for } e \in \mathscr{E}_\sigma, \sigma \in \mathscr{F}_K, K \in \mathscr{M}\}$$

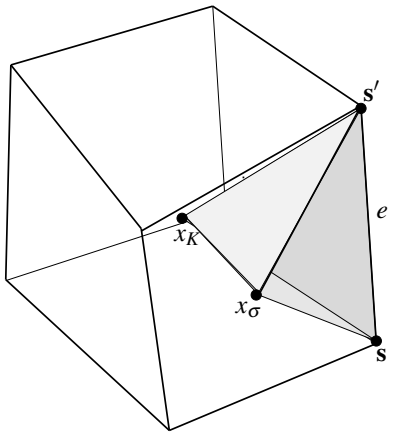


***Figure 1*** *Tetrahedron $T_{K,\sigma,e}$ of the sub-mesh $\mathscr{T}$.*

of the mesh $\mathscr{M}$, where $T_{K,\sigma,e}$ is the tetrahedron defined by the cell centre $x_K$ and the triangle $T_{\sigma,e}$ as shown by Figure 1.

For a given $v \in \widehat{W}_{\mathfrak{D}}$, we define the function $v_{\mathscr{T}} \in H^1(\Omega)$ as the continuous piecewise affine function on each tetrahedron $T$ of $\mathscr{T}$ such that $v_{\mathscr{T}}(x_K) = v_K$, $v_{\mathscr{T}}(\mathbf{s}) = v_{\mathbf{s}}$, and $v_{\mathscr{T}}(x_\sigma) = I_\sigma(v)$ for all $K \in \mathscr{M}$, $\mathbf{s} \in \mathscr{V}$, $\sigma \in \mathscr{F}$. The nodal basis of this finite element discretization will be denoted by $((\eta_K)_{K\in\mathscr{M}}, (\eta_{\mathbf{s}})_{\mathbf{s}\in\mathscr{V}})$.

Following [16], the VAG scheme is defined by the discrete variational formulation: find $u \in \widehat{W}_{\mathfrak{D}}$ such that $u_{\mathbf{s}} = u^D_{\mathbf{s}}$ for all $\mathbf{s} \in \mathscr{V}_{ext}$, and for all $v \in W_{\mathfrak{D}}$,

$$a_{\mathfrak{D}}(u,v) = \int_\Omega f(x)\, v_{\mathscr{T}}(x)\, dx,$$

where $a_{\mathfrak{D}}$ is the bilinear form defined by

$$a_{\mathfrak{D}}(u,v) = \int_\Omega \nabla u_{\mathscr{T}}(x) \cdot \Lambda(x)\, \nabla v_{\mathscr{T}}(x)\, dx$$

for all $(u,v) \in \widehat{W}_{\mathfrak{D}} \times \widehat{W}_{\mathfrak{D}}$, and

$$u^D_{\mathbf{s}} = \frac{1}{\int_{\partial\Omega} \eta_{\mathbf{s}}(x)\, d\sigma} \int_{\partial\Omega} u^D(x) \eta_{\mathbf{s}}(x)\, d\sigma$$

for all $\mathbf{s} \in \mathscr{V}_{ext}$.

*Conservative generalized fluxes*

Let us define for all $K \in \mathscr{M}$ and $\mathbf{s}, \mathbf{s}' \in \mathscr{V}_K$

$$a^{\mathbf{s}'}_{K,\mathbf{s}} = \int_K \nabla \eta_{\mathbf{s}}(x) \cdot \Lambda(x) \nabla \eta_{\mathbf{s}'}(x)\, dx. \tag{4}$$

One has

$$a_{\mathfrak{D}}(u,v) = \sum_{K\in\mathscr{M}} \sum_{\mathbf{s}\in\mathscr{V}_K} \sum_{\mathbf{s}'\in\mathscr{V}_K} a^{\mathbf{s}'}_{K,\mathbf{s}} (u_{\mathbf{s}'} - u_K)(v_{\mathbf{s}} - v_K),$$

leading to the definition of the following conservative generalized fluxes between a given cell $K \in \mathscr{M}$ and its vertices $\mathbf{s} \in \mathscr{V}_K$:

$$F_{K,\mathbf{s}}(u) = \sum_{\mathbf{s}'\in\mathscr{V}_K} a^{\mathbf{s}'}_{K,\mathbf{s}} (u_K - u_{\mathbf{s}'}), \tag{5}$$

and

$$F_{\mathbf{s},K}(u) = -F_{K,\mathbf{s}}(u). \tag{6}$$

The VAG scheme is equivalent to the following discrete system of balance equations:

$$\begin{cases} \displaystyle\sum_{\mathbf{s}\in\mathscr{V}_K} F_{K,\mathbf{s}}(u) = \int_K f(x)\ \eta_K(x)\ dx, & K\in\mathscr{M}, \\ \displaystyle\sum_{K\in\mathscr{M}_\mathbf{s}} F_{\mathbf{s},K}(u) = \int_\Omega f(x)\ \eta_\mathbf{s}(x)\ dx, & \mathbf{s}\in\mathscr{V}_{int}, \\ u_\mathbf{s} = u^D_\mathbf{s}, & \mathbf{s}\in\mathscr{V}_{ext}. \end{cases}$$

Let us notice, that the first equation in the above system involves for each cell $K$ the only cell unknown $u_K$. It results that the cell unknowns can be eliminated of the above system without any fill-in leading to a vertex centred scheme with typically a 27 points stencil on topologically Cartesian grids.

One may easily check that the VAG scheme generalized fluxes can be rewritten as follows:

$$F_{K,\mathbf{s}}(u) = \int_K -\Lambda(x)\nabla u_\mathscr{T}(x)\cdot\nabla\eta_\mathbf{s}(x)\ dx. \tag{7}$$

This formula provides in 2D an interpretation of the VAG scheme generalized fluxes as Control Volume Finite Element (CVFE) fluxes [9] on a triangular submesh. In 2D, $x_\sigma$ is chosen to be the mid-point of the edge $\sigma=\mathbf{s}\mathbf{s}'$, and the interpolation is simply defined by $I_\sigma(v)=\dfrac{v_\mathbf{s}+v_{\mathbf{s}'}}{2}$. It results that the triangular submesh $\mathscr{T}$ is rather defined in 2D as the set of triangles obtained for each cell $K$ by joining each face $\sigma$ of the cell $K$ to the cell centre $x_K$. Then, the VAG scheme reduces to the $\mathbb{P}_1$ finite element scheme on the submesh $\mathscr{T}$. Let $\mathbf{a}$ be the mid-point of $\mathbf{s}x_K$ (see figure 2). Using (7), one easily shows that, assuming a cellwise constant tensor field $\Lambda$, one has

$$F_{K,\mathbf{s}}(u) = \int_{\widehat{x_\sigma\mathbf{a}}\cup\widehat{x_{\sigma'}\mathbf{a}}} -\Lambda(x)\nabla u_\mathscr{T}(x)\cdot\mathbf{n}_K d\sigma,$$

where $\widehat{x_\sigma\mathbf{a}}$ (respectively $\widehat{x_{\sigma'}\mathbf{a}}$) is any curved segment inside the triangle $\sigma x_K$ (respectively $\sigma' x_K$) and $\mathbf{n}_K$ is the normal outward the CVFE control volume containing $x_K$ (see figure 2). The flexibility in the definition of the curved edges of the CVFE control volumes will be exploited in the next subsection to adapt the porous volume at the vertices and at the cell centres of the mesh in heterogeneous cases. This

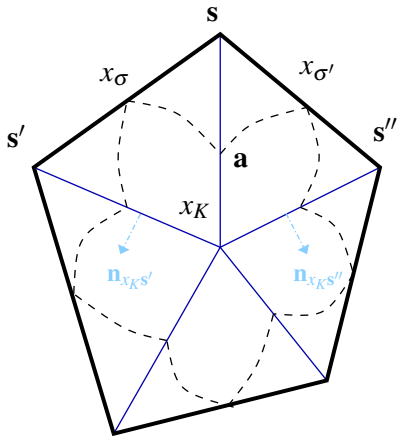


***Figure 2*** *CVFE interpretation of the fluxes $F_{K,\mathbf{s}}(u)$ in the 2D case.*

geometrical CVFE interpretation of the VAG generalized fluxes cannot be extended to the 3D case due to the interpolation at the face centres which has been used to avoid numerous additional unknowns at the faces.

*Application to a compositional multiphase Darcy flow model*

This subsection presents how to use the VAG scheme fluxes to discretize a compositional multiphase Darcy flow on a general mesh, following the framework described in the introduction by (1)-(3). Due to the previous definition of the VAG fluxes (5)-(6), the first idea is to define the set of control volumes $\mathscr{G}$ as the union of the cells and of the interior vertices

$$\mathscr{G} = \mathscr{M} \cup \mathscr{V}_{int}.$$

Remark that $\mathscr{G}$ must also include Neumann boundary vertices if this boundary condition is used in the problem, see [17]. Thus the flux from control volume $X = K$ to control volume $Y = \mathbf{s}$ is then given by

$$F_{X,Y}(u) = F_{K,\mathbf{s}}(u)\ ,\ \ \forall \mathbf{s} \in \mathscr{V}_K$$

and satisfies a MPFA formulation (1)-(2) due to (5) and (6). These generalized fluxes $F_{K,\mathbf{s}}(u)$, between a cell $K$ and its vertices $\mathbf{s} \in \mathscr{V}_K$, are then classically used for the approximation of the transport terms, in addition to an upwind scheme as briefly presented in (3).

Although these fluxes are not defined in the usual way, that is as the approximation of the continuous fluxes $\int_\sigma -\Lambda \nabla \bar{u} \cdot \mathbf{n}_\sigma d\sigma$ on a given face $\sigma$ of the mesh, the mathematical analysis developed in [18] shows that they lead to a convergent scheme, at least in a particular two-phase flow case. It is proved for the decoupled case where the sum of the mobilities is independent on the saturation, that the discrete saturation converges weakly in $L^\infty$ to the weak solution of the saturation equation. The proof follows the lines of [12] dealing with CVFE schemes (see also [13] for TPFA schemes) using a weak BV estimate for the VAG generalized fluxes together with the finite element variational formulation of the pressure equation.

Since a control volume is either a cell $K \in \mathscr{M}$ or a vertex $\mathbf{s} \in \mathscr{V}_{int}$, a porous volume $\Phi_X$ must be associated to each control volume $X \in \mathscr{G}$ such that

$$\sum_{X \in \mathscr{G}} \Phi_X = \int_\Omega \Phi(x) dx \text{ and } \Phi_X > 0 \text{ for all } X \in \mathscr{G}. \tag{8}$$

The method is based on a conservative redistribution to the vertices of the surrounding cell porous volumes

$$\Phi_X = \begin{cases} \omega \sum\limits_{K \in \mathscr{M}_\mathbf{s}} \alpha_K^\mathbf{s} \widetilde{\Phi}_K & \text{if } X = \mathbf{s} \in \mathscr{V}_{int}, \\ \\ \widetilde{\Phi}_K (1 - \omega \sum\limits_{\mathbf{s} \in \mathscr{V}_K \setminus \mathscr{V}_{ext}} \alpha_K^\mathbf{s}) & \text{if } X = K \in \mathscr{M}. \end{cases} \tag{9}$$

with $\widetilde{\Phi}_K = \int_K \Phi(x) dx$, and $\alpha_K^\mathbf{s} \geq 0$, $\sum_{K \in \mathscr{M}_\mathbf{s}} \alpha_K^\mathbf{s} = 1$, which guarantees (8) provided that the parameter $\omega > 0$ is chosen small enough. Moreover the main question is to associate to each vertex a porous volume in such a way that the components velocities are well approximated. Thus in practice, the weights $\alpha_K^\mathbf{s}$ are chosen in such a way that the porous volumes $\Phi_\mathbf{s}$ at the vertices are mainly taken from the surrounding cells with the highest permeabilities, using (4) and the formula:

$$\alpha_K^\mathbf{s} = \frac{a_{K,\mathbf{s}}}{\sum\limits_{K' \in \mathscr{M}_\mathbf{s}} a_{K',\mathbf{s}}}, \tag{10}$$

for all $\mathbf{s} \in \mathscr{V}_{int}$ and $K \in \mathscr{M}_\mathbf{s}$ with

$$a_{K,\mathbf{s}} = \sum_{\mathbf{s}' \in \mathscr{V}_K \setminus \mathscr{V}_{ext}} a_{K,\mathbf{s}}^{\mathbf{s}'} > 0.$$

This choice of the weights is the key ingredient to obtain an accurate approximation of the saturations and compositions on the coarse meshes which are used in practical situations involving highly heterogeneous

media. This point, as the influence of $\omega$, is discussed in the following section through various numerical tests.

Since the fluxes $F_{K,\mathbf{s}}(u)$ between the cell $K$ and its vertices $\mathbf{s}$ depend on the only cell unknown $u_K$, it is easily seen from (3) that all the cell unknowns can be eliminated from the Jacobian matrix of the multiphase system (3) without any fill-in (see [17] for details). It results that the VAG scheme typically leads to a 27 points stencil on topologically Cartesian grids as it is the case for cell centred schemes. On the other hand, it will clearly lead to a much sparser scheme than cell centred schemes on tetrahedral meshes as it will be shown in the numerical section below.

**Numerical examples**

*Two phase flow for a strongly heterogeneous test case on a coarse mesh*

The aim of the following test case is to show that, thanks to the redistribution of the porous volume at the vertices defined by (10), (9), the VAG scheme provides solutions which are just as accurate as the solutions given by cell centred schemes in the case of large jumps of the permeability tensor on coarse meshes.

Let us consider a stratified reservoir $\Omega = (0,100) \times (0,50) \times (0,100)$ m$^3$ with five horizontal layers $l = 1, \cdots, 5$ of thickness 20 m, and numbered by their increasing vertical position. The even layers are drains of constant high isotropic permeability $\Lambda_d$ and odd layers are barriers of constant isotropic low permeability $\Lambda_b$ with $\left|\frac{\Lambda_d}{\Lambda_b}\right| = 10^4$.

The fluid model is a simple immiscible incompressible two-phase (say gas ($g$) and water ($w$)) flow, no capillary effect, no gravity and the sum of the mobilities of both phases equal to one. Thus the model reduces to a hyperbolic equation for the gas saturation, still denoted by $S^g$, coupled to a fixed elliptic equation for the pressure $P$. The porosity $\Phi$ is constant, and the reservoir is initially saturated with water. A pressure $P_1$ is fixed at the left side $x = 0$ and a pressure $P_2$ at right side $x = 100$ such that $P_1 > P_2$. The input gas saturation is set to $S^g_D = 1$ at the input boundary $x = 0$. Homogeneous Neumann boundary conditions are imposed at the remaining boundaries. The mesh is a coarse uniform Cartesian grid of size $100 \times 1 \times 5$ with only one cell in the width of each layer as shown in Figure 3.

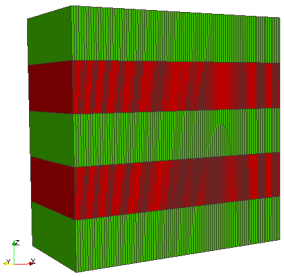

***Figure 3*** *Mesh and layering : drains (red color), barriers (green color).*

Figure 4 exhibits the evolution of the gas flow rate at the right boundary, using either the weights $\alpha^{\mathbf{s}}_K$ defined by (10) in subfigure 4(a) or the uniform weights $\alpha^{\mathbf{s}}_K = \frac{1}{\#\mathscr{M}_{\mathbf{s}}}$ in subfigure 4(b), where $\#\mathscr{M}_{\mathbf{s}}$ is the number of cells sharing the vertex $\mathbf{s}$. It is compared with the solution obtained with the TPFA scheme on both subfigures.

It clearly shows that the solution provided by the VAG scheme is independent on the parameter $\omega$ and matches the solution of the TPFA scheme for the choice of the weights (10). On the contrary, the gas breakthrough obtained by the VAG scheme with the uniform weights is clearly delayed when the

parameter $\omega$, i.e. the pore volume at the vertices, increases. This is due to the fact that the total pore volume defined by the cells of the drains plus the vertices at the interface between the drains and the barriers is roughly independent of $\omega$ in the first case but increases with the parameter $\omega$ in the second case.

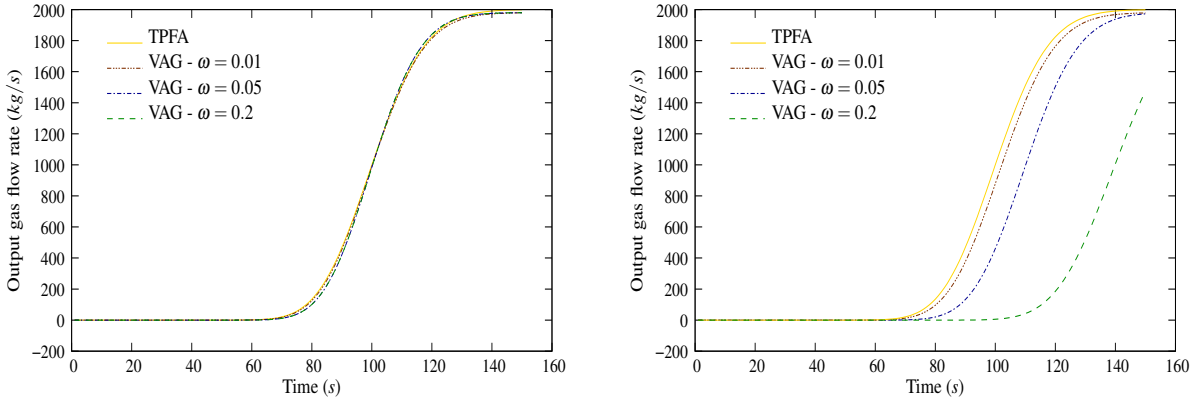


(a) $\alpha_K^{\mathbf{s}}$ defined by (10)

(b) $\alpha_K^{\mathbf{s}} = \dfrac{1}{\#\mathscr{M}_{\mathbf{s}}}$ with $\#\mathscr{M}_{\mathbf{s}}$ the number of cells sharing the vertex $\mathbf{s}$

***Figure 4*** *Gas flow rate at the right boundary function of time.*

*Two phase flow with discontinuous capillary pressures*

The objective of this 2D immiscible incompressible two phase (say oil ($o$) and water ($w$)) flow test case is to assess the ability of the VAG scheme to deal with different rocktypes. In such cases, the main issue is how to define a capillary pressure (and similarly relative permeabilities) for each nodal control volume in order to allow for discontinuous saturations at the interface between two rocktypes.

The solution of this problem relies again on the flexibility of the VAG scheme in the definition of the porous volumes at the vertices. The rocktypes are denoted by $\mathrm{rt}_K$ for each cell $K \in \mathscr{M}$. For each node $\mathbf{s} \in \mathscr{V}_{int}$ we choose a rocktype $\mathrm{rt}_{\mathbf{s}} = \mathrm{rt}_{K_{\mathbf{s}}}$ with $K_{\mathbf{s}} \in \mathrm{argmax}\{a_{K,\mathbf{s}},\, K \in \mathscr{M}_{\mathbf{s}}\}$ and we set

$$\mathscr{N}_{\mathbf{s}} = \{K \in \mathscr{M}_{\mathbf{s}} \,|\, \mathrm{rt}_K = \mathrm{rt}_{K_{\mathbf{s}}}\}.$$

The porous volumes (9) are defined with the following new definition of the weights (10) in such a way that the porous volume at the vertex $\mathbf{s}$ is taken only from the cells with the same rocktype $\mathrm{rt}_{K_{\mathbf{s}}}$.

$$\alpha_K^{\mathbf{s}} = \begin{cases} \dfrac{a_{K,\mathbf{s}}}{\displaystyle\sum_{K' \in \mathscr{N}_{\mathbf{s}}} a_{K',\mathbf{s}}} & \text{if } \mathbf{s} \in \mathscr{N}_{\mathbf{s}}, \\ 0 & \text{else .} \end{cases} \tag{11}$$

In the following test case, the domain $\Omega = (0,100) \times (0,100)$ in the $(x,z)$ plane is split into two layers $\Omega_1 = (0,100) \times (0,50)$ and $\Omega_2 = (0,100) \times (50,100)$, each corresponding to a rocktype $\mathrm{rt} = 1$ and 2 respectively. The porosity $\Phi = 0.1$, and the permeability $\Lambda = 10^{-12} I$ are homogeneous and the same for both rocktypes. The relative permeabilities are set to $k_{r,\alpha}(S^\alpha) = S^\alpha$, $\alpha = o, w$, for both rocktypes while the capillary pressure of each rocktype is defined by

$$P_{c,\mathrm{rt}}(S^o) = a_{\mathrm{rt}} S^o + b_{\mathrm{rt}}$$

with $a_1 = a_2 = 10^{+5}$, $b_1 = 0$ and $b_2 = 0.5\ 10^{+5}$. Homogeneous Neumann boundary conditions are imposed at the boundary of $\Omega$ and the flow is buoyancy driven starting from the initial oil saturation

defined by

$$S^o(x) = \begin{cases} 0.3 & \text{if } x \in \Omega_1, \\ 0 & \text{if } x \in \Omega_2. \end{cases}$$

Figures 5 and 6 compare at two different times the solutions obtained for the oil saturation along the z axis on the coarse grid $2 \times 10$ and on the fine grid $16 \times 80$ with the TPFA scheme and with three different VAG schemes. Since the permeability is homogeneous and the mesh uniform, there are two possible choices for the rocktypes at the vertices located at the interfaces between the two subdomains. The VAGs1 scheme (respectively VAGs2) is the one obtained with the choice of the rocktype 1 (respectively 2) at the interface between the two subdomains. The VAGa scheme is obtained with the weights defined by (10) and with a capillary pressure at the interfaces given by an harmonic average of both rocktype capillary pressures. In all cases, the parameter $\omega$ is computed such that the minimum porous volumes at vertices and at cells match.

Note that the discrete solutions are in all cases independent on $x$ although the VAG scheme does not degenerate to a 1D scheme while the TPFA scheme does for this test case. For the VAG schemes the following post-processed values of the oil saturation are plotted at the cell centre $z_K$ along the z axis:

$$\tilde{S}_K^o = (1 - \omega \sum_{\mathbf{s} \in \mathscr{V}_K \setminus \mathscr{V}_{ext}} \alpha_K^{\mathbf{s}}) S_K^o + \omega \sum_{\mathbf{s} \in \mathscr{V}_K \setminus \mathscr{V}_{ext}} \alpha_K^{\mathbf{s}} S_{\mathbf{s}}^o.$$

It is known that oil can only flow by gravity to the top subdomain provided that the capillary pressures can achieve continuity at the interface, meaning here that the jump of the oil saturation at the interface must reach the value 0.5. It can be checked that it is the case for all schemes on the fine grid solution. On the coarse grid, the VAGs1 and TPFA scheme are very close, the VAGs2 scheme is slightly better, while the VAGa scheme, as could be expected, is much worse in capturing the saturation jump.

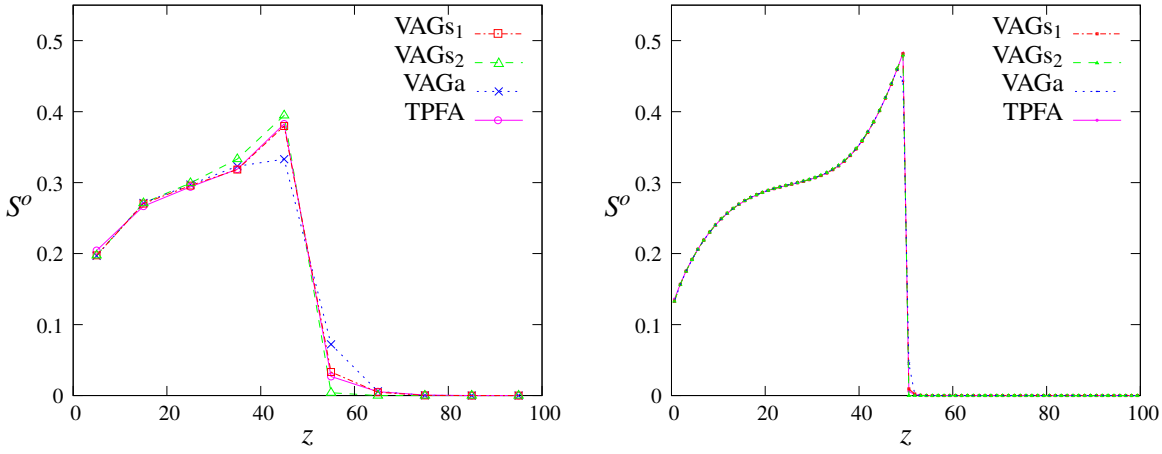


(a) grid $2 \times 10$ (b) grid $16 \times 80$

***Figure 5*** *Oil saturation along the z axis after* 15 *days of simulation on the coarse and fine grids, and for the TPFA, VAGs1, VGAs2, and VAGa schemes.*

*Numerical diffusion and CPU time for a decoupled two phase flow*

We consider a simple immiscible incompressible two-phase (say $CO_2(g)$) and water ($w$)) flow, no capillary effect, no gravity and the sum of the mobilities of both phases equal to one. In such a case, the model reduces to a linear scalar hyperbolic equation for the gas saturation denoted by $S^g$ coupled to an elliptic equation for the pressure $P$. The simulation is done on the domain $\Omega = (0,1)^3$ with the permeability tensor $\Lambda = I$, a porosity $\Phi = 1$, and the initial gas saturation $S^g(x,0) = 0$. Let $(x,y,z)$ denote the Cartesian coordinates of $x$. We specify a pressure $P_1$ at the left side $x = 0$ and a pressure $P_2$ at right side $x = 1$ such that $P_1 > P_2$. Homogeneous Neumann boundary conditions are imposed at the remaining

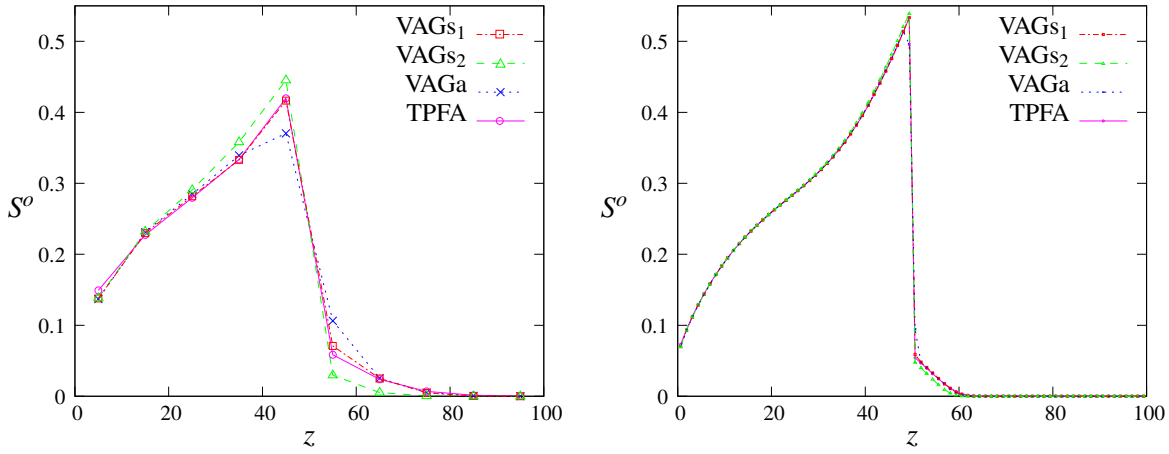


(a) grid $2 \times 10$ (b) grid $16 \times 80$

***Figure 6*** *Oil saturation along the z axis after* 30 *days of simulation on the coarse and fine grids, and for the TPFA, VAGs1, VGAs2, and VAGa schemes.*

boundaries. The input gas saturation is set to $S_D^g = 1$ at the input boundary $x = 0$. The system admits an analytical solution given by

$$P(x) = (P_2 - P_1)\, x + P_1,$$

and

$$S^g(x,t) = \begin{cases} 1 & \text{if } x \leqslant (P_1 - P_2)\, t, \\ 0 & \text{else.} \end{cases}$$

We consider two different grids for this test. The first one is a uniform Cartesian grid of size $32 \times 32 \times 32$. The second grid is composed of 15266 tetrahedra. Both meshes are extracted from the FVCA6 3D Benchmark [19]. Figure 7 shows, for each grid, the projection of the gas saturation $S^g$ on the $x$–coordinate axis at the simulation time for which the gas has filled half of the reservoir. We have plotted the analytical solution $S^g$ and the discrete solutions $(x_K, S_K^g)$ for all cells $K \in \mathscr{M}$ obtained with the VAG and the MPFA O schemes. For the VAG scheme we use the post-processed values,

$$\tilde{S}_K^g = (1 - \omega \sum_{\mathbf{s} \in \mathscr{V}_K \setminus \mathscr{V}_{ext}} \alpha_K^{\mathbf{s}}) S_K^g + \omega \sum_{\mathbf{s} \in \mathscr{V}_K \setminus \mathscr{V}_{ext}} \alpha_K^{\mathbf{s}} S_{\mathbf{s}}^g$$

deduced from the redistribution of the volumes defined by (9)-(10) .

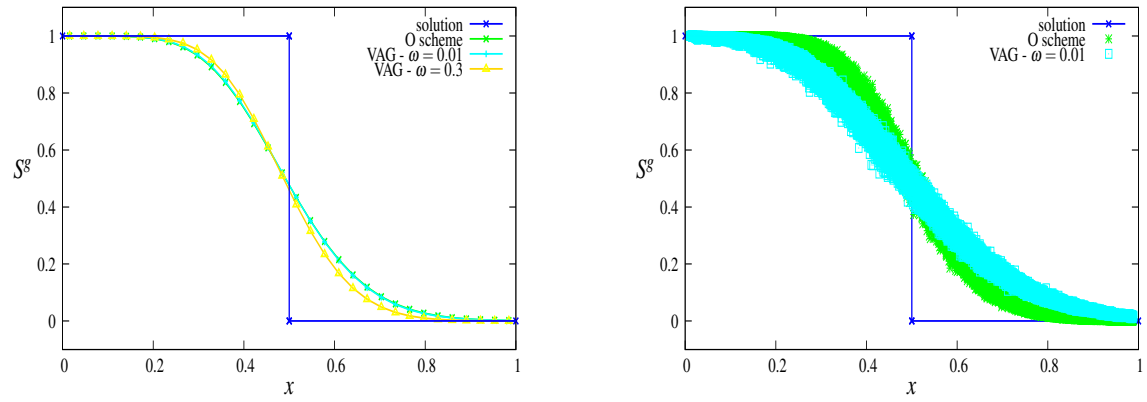


(a) Hexahedral mesh (b) Tetrahedral mesh

***Figure 7*** *Propagation in the horizontal direction of the gas saturation.*

The results presented in Figure 7 clearly show that, for each grid, the discrete solutions of both schemes intersect the analytical solution at the point $(\frac{1}{2},\frac{1}{2})$, which exhibits that the velocity of the flow is well approximated. On Figure 7(a), the solutions of the VAG scheme on the Cartesian grid is plotted for both $\omega = 0.01$ and $\omega = 0.3$ (9). The value $\omega = 0.3$ roughly corresponds to match the pore volume of each vertex $\phi_{\mathbf{s}}$ with the pore volume of each surrounding cell $\phi_K$, $K \in \mathscr{M}_{\mathbf{s}}$. As expected, the choice $\omega = 0.3$ leads to a slightly less diffusive scheme than the VAG scheme with $\omega = 0.01$. We note also that the VAG scheme is slightly less diffusive on such meshes than the MPFA O scheme (which degenerates for Cartesian grids to the TPFA scheme). On the other hand, for the tetrahedral mesh, we can notice on Figure 7(b) that the VAG scheme is slightly more diffusive than the MPFA O scheme. This has been observed for both values of $\omega = 0.01$ and 0.3. Note also that for both type of meshes the convergence of the VAG scheme has been obtained numerically for both $\omega = 0.01$ and $\omega = 0.3$.

In terms of CPU time a ratio of 15 is observed between the simulation time obtained with the MPFA O scheme on the tetrahedral mesh and the VAG scheme on the same mesh. This huge factor is due to the reduced size of the linear system obtained with the VAG scheme after elimination of the cell unknowns compared with the MPFA O scheme, both in terms of number of unknowns (around five time less for the VAG scheme than for the MPFA O scheme) and in terms of number of non zero elements per line.

*$CO_2$ injection with dissolution and vaporization of $H_2O$ and salt precipitation*

This test case simulates the nearwell injection of $CO_2$ in a saline aquifer. Due to the vaporization of $H_2O$ in the gas phase, the water phase is drying in the nearwell region leading to the precipitation of the salt dissolved in the water phase. This may result in a reduction of the nearwell permeability. This phenomenon could for example explain the loss of injectivity observed in the Tubaen saline aquifer of the Snohvit field in the Barents sea where around 700000 tons of $CO_2$ are injected each year since 2008.

The model is a three phases (gas ($g$), water ($w$), mineral ($m$)) three components ($CO_2$, $H_2O$, *salt*) ) compositional Darcy flow. It is assumed that the $H_2O$ component can vaporize in the gas phase and that the $CO_2$ and *salt* components can dissolve in the water phase. It results that $\mathscr{C}^w = \{H_2O, CO_2, salt\}$, $\mathscr{C}^g = \{H_2O, CO_2\}$, and $\mathscr{C}^m = \{salt\}$ where $\mathscr{C}^\alpha$ denotes the set of components may be present in the phase $\alpha$. The mineral phase is immobile with a null relative permeability $k_{r,m} = 0$, and the water and gas phase relative permeabilities $k_{r,\alpha}$ are non decreasing functions of the reduced saturation $\widehat{S}^\alpha = \dfrac{S^\alpha}{S^w + S^g}$, $\alpha = w, g$.

$$k_{r,\alpha}(\widehat{S}^\alpha) = \begin{cases} \left(\dfrac{\widehat{S}^\alpha - S_{r,\alpha}}{1 - S_{r,\alpha}}\right)^{e^\alpha} & \text{if } \widehat{S}^\alpha \in [S_{r,\alpha}, 1] \\ 0 & \text{if } \widehat{S}^\alpha < S_{r,\alpha}, \end{cases}$$

with $e^w = 5$, $e^g = 2$, $S_{r,w} = 0.3$ and $S_{r,g} = 0$. The reference pressure is chosen to be the gas pressure $P = P^g$, and we set $P^w = P^g + P_{c,w}(\widehat{S}^w)$ with

$$P_{c,w}(\widehat{S}^w) = P_{c,1} \log\left(\frac{\widehat{S}^w - S_{r,w}}{1 - S_{r,w}}\right) - P_{c,2},$$

for $1 \geq \widehat{S}_w > S_{r,w}$, where $P_{c,1} = 2.10^4$ Pa, $P_{c,2} = 10^4$ Pa. The thermodynamical equilibrium is modelled by equilibrium constants $H_i$ of the component $i$ such that

$$\begin{cases} C^g_{H_2O} = H_{H_2O}\, C^w_{H_2O} & \text{in presence of both phases } w \text{ and } g, \\ C^w_{CO_2} = H_{CO_2}\, C^g_{CO_2} & \text{in presence of both phases } w \text{ and } g, \\ C^w_{salt} = H_{salt} & \text{in presence of both phases } w \text{ and } m. \end{cases}$$

where $C^\alpha_i$ is the molar concentration of the component $i$ in the phase $\alpha$. The equilibrium constants will be considered fixed in the range of pressure and temperature with the following values $H_{H_2O} = 0.025$,

$H_{CO_2} = 0.03$ and $H_{salt} = 0.39$ in $kg/kg$. Let us also denote the total molar fractions of the component $i$ by $Z_i$ and by $Z = (Z_i)_i$ the vector of the total molar fractions. With these assumptions, the thermodynamical flash, which gives the phases present, admits an analytical solution, independent of the pressure $P$, and with entries $Z$ in the two dimensional simplex

$$\{(Z_{CO_2}, Z_{salt}) \,|\, Z_{CO_2} \geq 0, Z_{salt} \geq 0, 1 - Z_{CO_2} - Z_{salt} \geq 0\}.$$

The solution is exhibited Figure 8 where we have set

$$E_1 = (E_{CO_2}\, H_{CO_2}, 0), \quad E_2 = (E_{CO_2}, 0), \quad E_3 = (D_{CO_2}, 0), \quad E_4 = (0, H_{salt}), \quad E_5 = (H_{CO_2}\, D_{CO_2}, H_{salt}),$$

with $D_{CO_2} = \dfrac{1 - H_{H_2O}\,(1 - H_{salt})}{1 - H_{H_2O}\, H_{CO_2}}$ and $E_{CO_2} = \dfrac{1 - H_{H_2O}}{1 - H_{H_2O}\, H_{CO_2}}$.

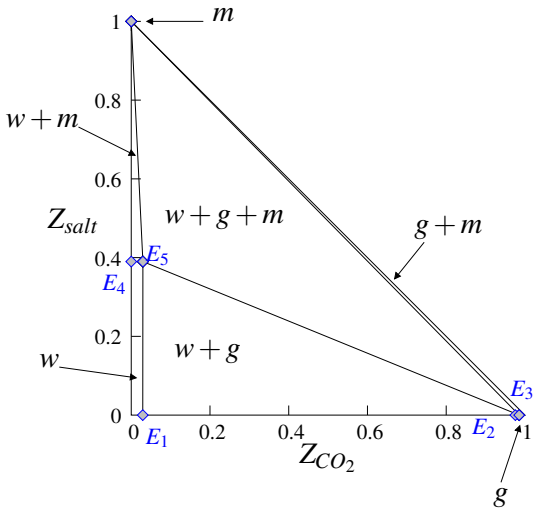


***Figure 8*** *Diagram of present phases in the space* $(Z_{CO_2}, Z_{salt})$.

The 3D nearwell grids used for the simulation are exhibited in Figure 9. The first step of the discretization is to create a radial mesh, Figure 9(a), that is exponentially refined down to the well boundary. This nearwell radial local refinement is matched with the reservoir $\Omega = (-15, 15) \times (-15, 15) \times (-7.5, 7.5)$ $m^3$ using either hexahedra (see Figure 9(b)) or both tetrahedra and pyramids, (see Figure 9(c)). The radius of the well is 10 cm and the radius of the radial zone is 5 m. The well is deviated by an angle of 20 degrees away from the vertical axis $z$ in the $x,z$ plane. The hexahedral grid has 42633 cells and the hybrid grid 77599 cells.

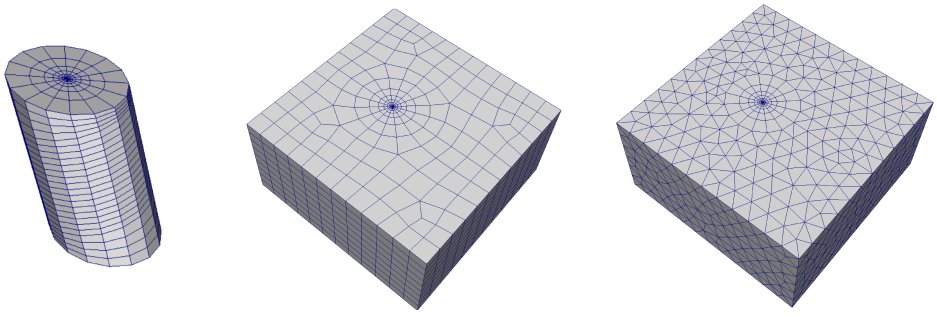

(a) exponentially refined radial mesh

(b) unstructured mesh with only hexahedra

(c) hybrid mesh with hexahedra, tetrahedra and pyramids

***Figure 9*** *Nearwell meshes.*

The remaining of the data set and the boundary and initial conditions are the following. The porosity is set to $\Phi = 0.2$, and the permeability tensor $\Lambda$ is homogeneous and isotropic equal to 1. $10^{-12}$ $m^2$. The

density and the viscosity of the water phase are computed by correlations function of $P$ and $C^w$, and those of the gas phase by linear interpolation in the pressure $P$, the density of the mineral phase is fixed to $\rho^m = 2173$ kg/l.

Homogeneous Neumann boundary conditions are imposed on the top and bottom boundaries. Along the well boundary we impose the pressure $P(x,y,z) = P_{\text{well}} - \rho^g \parallel \mathbf{g} \parallel z$, with $P_{\text{well}} = 300\ 10^{+5}$ Pa, the input phase $S^g = 1$ and its composition $C^g_{CO_2} = 1$, $C^g_{H_2O} = 0$. On the lateral outer boundaries (resp. at initial time) the following hydrostatic pressure is imposed $P(x,y,z) = P_1 - \rho_l \parallel \mathbf{g} \parallel z$, with $P_1 = P_{\text{well}} - 10^{+5}$ Pa, as well as the following input (resp. initial) phase and its composition $S^w = 1$, $C^w_{H_2O} = 0.84$ and $C^w_{salt} = 0.16$.

The simulation time is fixed to 7 days in order to obtain a precipitation of the mineral up to around half of the radial zone. To avoid too small control volumes in the nearwell region, the parameter $\omega$ has been chosen in such a way that $\min_{K\in\mathscr{M}} \Phi_K = \min_{\mathbf{s}\in\mathscr{V}} \Phi_{\mathbf{s}}$, leading in our case to $\omega \sim 0.4$.

We report in the table 1 below for both schemes and for both meshes the number of unknowns *nu* ($\#\mathscr{M}$ for the MPFA O scheme and $\#\mathscr{V}_{int}$ for the VAG scheme), the number *nnz* of nonzeros blocks in the Jacobian after elimination of the cell unknowns for the VAG scheme, the average number of Newton iterations per time step *nnl*, and the average number of GMRES iterations per Newton step *nl*. The stopping criteria in terms of relative residual for both the Newton convergence and the linear convergence are set to $10^{-6}$. Note that the simulation with the MPFA O scheme on the hybrid mesh could not be obtained due to too high memory requirement for the matrix storage. The slight increase of nonlinear iterations between the MPFA and the VAG scheme and between both meshes, as seen in table 1, is probably due to the decrease of the control volume sizes.

| Mesh-Scheme | *nu* | *nnz* | *nnl* | *nl* |
|---|---|---|---|---|
| Hexahedral-MPFA | 42633 | 1100865 | 4.5 | 33 |
| Hexahedral-VAG | 42756 | 1103310 | 4.8 | 35 |
| Hybrid-MPFA | 77599 | 4092027 | - | - |
| Hybrid-VAG | 37833 | 884577 | 5.4 | 38 |

***Table 1*** *For both schemes and both meshes: number of unknowns nu, number nnz of nonzeros blocks in the Jacobian, average number nnl of Newton iterations per time step, and average number nl of GMRES iterations per Newton step.*

Figure 10 exhibits, for the two schemes and on both grids, the rate of variation of the masses of $CO_2$ and of the mineral in the reservoir function of time. We can notice that the VAG scheme solutions on both meshes are almost the same and only slightly differ from the O scheme solution. The oscillations observed in Figure 10(b) are a well-known phenomenon due to the appearance of the mineral phase on each successive cells when the *salt* reaches its maximum solubility.

Figure 11 exhibits the trajectory of the total mass fraction $Z$ in the simplex $(Z_{CO_2}, Z_{salt})$ function of time for four cells $K_i$, $i = 1,\cdots,4$. Starting from an initial state given by a single water phase and $Z_{CO_2} = 0$, the mass of $CO_2$ increases due to the injection. The $CO_2$ is initially fully dissolved in the water phase, then the gas phase appears and its mass fraction $\theta^g$ increases. As long as $C^w_{Salt}$ is roughly constant, the trajectory $Z$ is close to the line defined by

$$\begin{cases} Z_{CO_2} = (1-\theta^g)C^w_{CO_2} + \theta^g C^g_{CO_2}, \\ Z_{salt} = (1-\theta^g)C^w_{salt} \end{cases}$$

since $C^w_{CO_2}$ and $C^g_{CO_2}$ are both fixed by $C^w_{salt}$ and the thermodynamical equilibrium constants. Once the water saturation $S^w$ is close to the irreducible water saturation $S_{r,w}$, the composition $C^w_{salt}$ increases

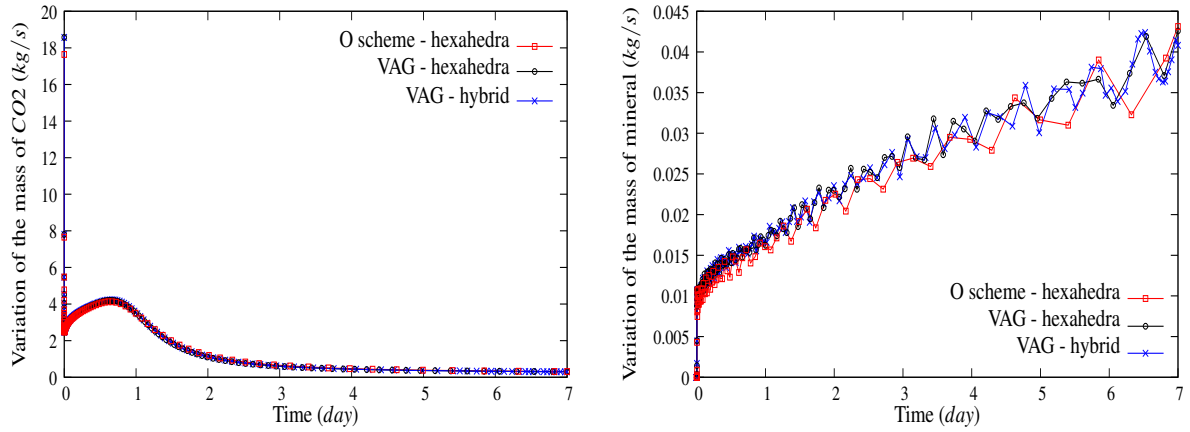


(a) $CO_2$ (b) Mineral

***Figure 10*** *Rate of variation of the mass of $CO_2$ and of mineral in the reservoir function of time.*

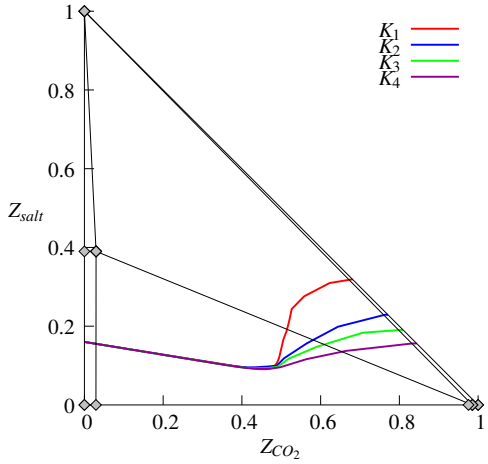


***Figure 11*** *Trajectory of $Z_K$ for four cells $K_i$, $i = 1, \cdots, 4$ in the space $(Z_{CO_2}, Z_{salt})$. The four cells at all at $z = -7$ m and ordered according to their increasing distance to the well axis.*

rapidly due to the vaporization of $H_2O$ and the mineral phase appears. At the end of the simulation, $CO_2$ is the only remaining component in the gas phase and the *salt* component in the mineral phase and the trajectory ends on the segment $Z_{H_2O} = 0$.

Figure 12(a) shows the water saturation at the end of the simulation, illustrating the nearwell drying. The precipitation of the salt is exhibited in Figure 12(b) where the mineral saturation higher than 0.1 percent is plotted at the end of the simulation. We can observe on Figure 12(c) the peak of mineral saturation around the well which is due to the reflux of the water phase close to the well by capillary effect. These results obtained with the VAG scheme on the hexahedral grid are similar to those obtained with the VAG scheme on the hybrid grid and to those obtained with the O scheme on the hexahedral grid.

## Conclusions

The above numerical results show that the VAG scheme seems to be an efficient scheme for multiphase flow simulation. Its space discretization is a combination of finite element and finite volume. It applies to general meshes, which may be possibly non conforming and with non planar faces and leads to a vertex-centred compact scheme after elimination of the cell unknowns in the linear system arising from the Newton linearization. Compared with usual finite element approaches, the VAG scheme has the ability to deal with highly heterogeneous media and different rocktypes on coarse meshes due to its

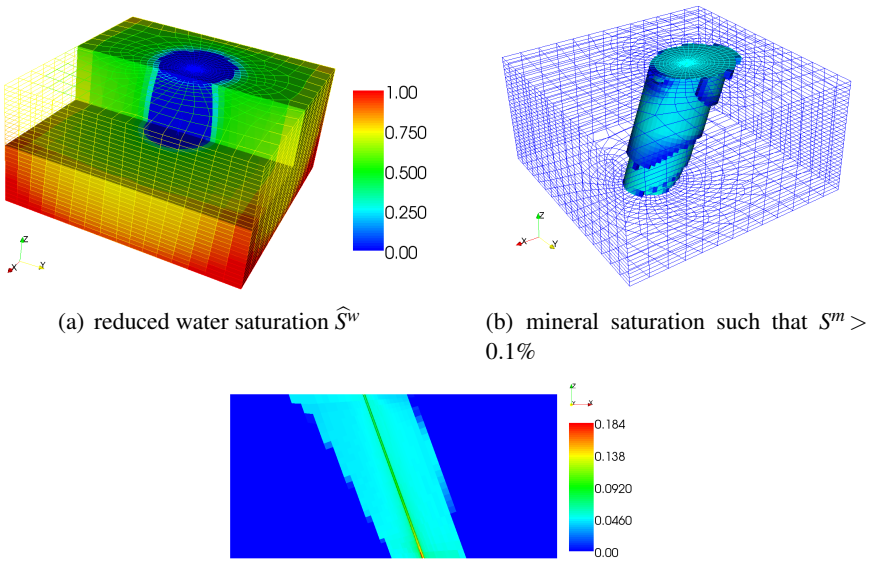


(a) reduced water saturation $\widehat{S}^w$

(b) mineral saturation such that $S^m > 0.1\%$

(c) Cut of the mineral saturation $S^m$

***Figure 12*** *Saturations at the end of the simulation.*

flexibility in the definition of the porous volumes at the vertices.

The efficiency of our approach on complex meshes and for complex compositional models is exhibited on three phases three components models which simulate the nearwell injection of miscible $CO_2$ in a saline aquifer taking into account the vaporization of $H_2O$ in the gas phase as well a the deposition of the salt.

In order to better take into account discontinuous capillary pressures, a more advanced solution, following the recent work [8], would be to consider as vertex unknowns the capillary pressures rather than the saturations, in such a way that the saturations at the vertices would be allowed to be discontinuous. This approach will be developed in a future work.

## Acknowledgments

The authors thank ANR VFSitCom, the COFFEE project of INRIA Sophia Antipolis, GNR MOMAS and TOTAL for partially supported this work and TOTAL for permission to publish it.

## References

[1] Aavatsmark, I., Barkve, T., Boe, O. and Mannseth, T. [1996] Discretization on non-orthogonal, quadrilateral grids for inhomogeneous, anisotropic media. *Journal of computational physics*, **127**(1), 2–14.
[2] Aavatsmark, I., Barkve, T., Boe, O. and Mannseth, T. [1998] Discretization on unstructured grids for inhomogeneous, anisotropic media. part 1: Derivation of the methods. *SIAM Journal on Scientific Computing*, **19**, 1700.
[3] Aavatsmark, I., Eigestad, G., Mallison, B. and Nordbotten, J. [2008] A compact multipoint flux approximation method with improved robustness. *Numerical Methods for Partial Differential Equations*, **24**(5), 1329–1360.
[4] Agélas, L., Di Pietro, D. and Droniou, J. [2010] The g method for heterogeneous anisotropic diffusion on general meshes. *Mathematical Modelling and Numerical Analysis*, **44**(4), 597–625.
[5] Agélas, L., Di Pietro, D., Eymard, R. and Masson, R. [2010] An abstract analysis framework for nonconforming approximations of diffusion on general meshes. *International Journal on Finite Volumes*, **7**(1).
[6] Agélas, L., Guichard, C. and Masson, R. [2010] Convergence of finite volume mpfa o type schemes for heterogeneous anisotropic diffusion problems on general meshes. *International Journal on Finite Volumes*, **7**(2).
[7] Aziz, K. and Settari, A. [1979] *Petroleum reservoir simulation*. Applied Science Publishers.
[8] Brenner, K., Cances, C. and Hilhorst, D. [2011] A convergent finite volume scheme for two-phase flows in porous media with discontinuous capillary pressure field. *Finite Volumes for Complex Applications VI-*

*Problems & Perspectives*, 185–193.
[9] Chen, Z. [2006] On the control volume finite element methods and their applications to multiphase flow. *Networks and Heterogeneous Media*, **1**(4), 689.
[10] Edwards, M. and Rogers, C. [1994] A flux continuous scheme for the full tensor pressure equation. *Proceedings of ECMOR IV–4th European Conference on the Mathematics of Oil Recovery, EAGE, Roros, Norway*.
[11] Edwards, M. and Rogers, C. [1998] Finite volume discretization with imposed flux continuity for the general tensor pressure equation. *Computational Geosciences*, **2**(4), 259–290.
[12] Eymard, R. and Gallouët, T. [1993] Convergence d'un schéma de type éléments finis-volumes finis pour un système formé d'une équation elliptique et d'une équation hyperbolique. *Modélisation mathématique et analyse numérique*, **27**(7), 843–861.
[13] Eymard, R., Gallouët, T. and Herbin, R. [2000] Finite volume methods. *Handbook of numerical analysis*, **7**, 713–1018.
[14] Eymard, R., Gallouët, T. and Herbin, R. [2010] Discretization of heterogeneous and anisotropic diffusion problems on general nonconforming meshes sushi: a scheme using stabilization and hybrid interfaces. *IMA Journal of Numerical Analysis*, **30**(4), 1009–1043.
[15] Eymard, R., Guichard, C. and Herbin, R. [2011] Benchmark 3d: the vag scheme. *Finite Volumes for Complex Applications VI – Problems and Persepectives*, Springer Proceedings in Mathematics, vol. 2, 213–222.
[16] Eymard, R., Guichard, C. and Herbin, R. [2012] Small-stencil 3d schemes for diffusive flows in porous media. *ESAIM: Mathematical Modelling and Numerical Analysis*, **46**(02), 265–290.
[17] Eymard, R., Guichard, C., Herbin, R. and Masson, R. [2012] Vertex centred discretization of multiphase compositional darcy flows on general meshes. *Computational Geosciences*, 1–19, ISSN 1420-0597.
[18] Eymard, R., Guichard, C., Herbin, R. and Masson, R. [2012] Vertex centred discretization of two-phase darcy flows on general meshes. *ESAIM: Proc.*, **35**.
[19] Eymard, R., Henry, G., Herbin, R., Hubert, F., Klöfkorn, R. and Manzini, G. [2011] 3d benchmark on discretization schemes for anisotropic diffusion problems on general grids. *Finite Volumes for Complex Applications VI-Problems & Perspectives*, 895–930.
[20] Huber, R. and Helmig, R. [2000] Node-centered finite volume discretizations for the numerical simulation of multiphase flow in heterogeneous porous media. *Computational Geosciences*, 141–164, ISSN 4.
[21] Peaceman, D. [1977] *Fundamentals of numerical reservoir simulation*, vol. 6. Elsevier.